JGR Atmospheres

RESEARCH ARTICLE
10.1029/2022JD038233

Special Section:
Land-atmosphere coupling: measurement, modelling and analysis

Revealing the Formation of the Dipole Mode of Eurasian Snow Cover Variability During Late Autumn

Taotao Zhang[1,2], Yingying Feng[3], and Haishan Chen[1,2]

[1]Key Laboratory of Meteorological Disaster, Ministry of Education (KLME)/International Joint Research Laboratory of Climate and Environment Change (ILCEC)/Collaborative Innovation Center on Forecast and Evaluation of Meteorological Disasters (CIC-FEMD), Nanjing University of Information Science & Technology (NUIST), Nanjing, China, [2]School of Atmospheric Sciences, NUIST, Nanjing, China, [3]State Key Laboratory of Tibetan Plateau Earth System and Resources Environment (TPESRE), Institute of Tibetan Plateau Research, Chinese Academy of Sciences, Beijing, China

Abstract A zonal dipole pattern of the interannual variability of Eurasian snow cover during late autumn has attracted growing interest due to its extensive influences on large-scale atmospheric circulations and climate anomalies, but it remains unknown what influences the formation of this pattern. This study revealed the potential drivers and the related physical processes of the dipole mode of the snow cover variability during 1979–2018. Results showed that the atmospheric circulation anomalies play a crucial role in forming the dipole mode, which could be further attributed to the influences of the atmospheric teleconnection patterns and the variations of sea surface temperature (SST) and sea ice concentration. Specifically, the anomalous circulations related to the teleconnections of the Eastern Atlantic pattern, East Atlantic–Western Russia pattern, and Scandinavian pattern could lead to the anomalies of air temperature and snowfall that directly shape the variability of snow cover. In addition, a dipole structure of the SST anomalies over the North Atlantic exerts an important effect on the snow cover variability through exciting an eastward propagating Rossby wave train prevailing over Eurasia. Moreover, the snow cover variability is closely linked to the sea ice variations over the Barents Sea that can regulate the anomalous circulations over Eurasia by altering the atmospheric dynamic and thermodynamic conditions. These influencing factors jointly account for about 66% of variances in the dipole mode of snow cover variability, suggesting that our findings can substantially improve the understanding of the Eurasian snow cover variations.

Plain Language Summary This study investigated the possible influencing factors responsible for the formation of the west-east dipole structure of Eurasian snow cover variability during late autumn that has notable impacts on the atmospheric circulations and climate anomalies in the following season. Results suggested that the anomalous circulations associated with the atmospheric teleconnections of the Eastern Atlantic pattern, East Atlantic-Western Russia pattern, and Scandinavian pattern can effectively regulate the snow cover variability related to the dipole pattern through inducing the anomalies of surface air temperature and snowfall. In addition, the North Atlantic sea surface temperature anomalies play a considerable role in forming the dipole mode by exciting a wave train type anomalous circulation over Eurasia. Furthermore, the variations of sea ice concentration in the Barents Sea could lead to the snow cover variability through modulating the temperature gradient over mid-high latitudes and the resultant circulation anomalies over Eurasia. The synergetic effect of these influencing factors explains about two-thirds of the snow cover variability related to the dipole mode, indicating the important contribution of our results to understanding the Eurasian autumn snow cover anomaly.

Key Points:

- The west-east dipole pattern is the intrinsic mode of the Eurasian snow cover variability during late autumn
- The dipole mode is closely associated with the Eastern Atlantic pattern, East Atlantic-Western Russia pattern, and Scandinavian pattern
- Anomalies of North Atlantic sea surface temperature and Barents sea ice can exert considerable effects on the dipole mode

Supporting Information:

Supporting Information may be found in the online version of this article.

Correspondence to:

T. Zhang,
ttzhang@nuist.edu.cn

Citation:

Zhang, T., Feng, Y., & Chen, H. (2023). Revealing the formation of the dipole mode of Eurasian snow cover variability during late autumn. *Journal of Geophysical Research: Atmospheres*, *128*, e2022JD038233. https://doi.org/10.1029/2022JD038233

Received 21 NOV 2022
Accepted 27 FEB 2023

1. Introduction

Seasonal snow cover is one of the most variable land surface components, which is extremely sensitive to climate change and in turn, could exert profound impacts on the atmosphere through the snow-albedo effect and the snow-hydrological effect (Barnett et al., 1988; Cohen & Rind, 1991; Groisman et al., 1994; Halder & Dirmeyer, 2017; Henderson et al., 2018; Xu & Dirmeyer, 2013). Previous studies have usually paid more attention to Eurasian snow cover variability during boreal spring owing to its significant impact on Asian summer monsoon precipitation (Halder & Dirmeyer, 2017; Peings & Douville, 2010; Wu & Kirtman, 2007; Wu et al., 2009; Zhang, Wang, Feng, et al., 2021; Zhang et al., 2017, 2019). Recently, an increasing number of studies have recognized that Eurasian snow cover during autumn can also effectively regulate large-scale anom-

alous atmospheric circulations during winter, which are the crucial contributors to winter climate variabilities, especially the extreme cold events, over the northern middle latitudes (Cohen et al., 2021; Douville et al., 2017; Furtado et al., 2015; Henderson et al., 2018; Luo & Wang, 2019; Peings et al., 2013). Therefore, a comprehensive understanding of the variabilities and the underlying drivers of Eurasian snow cover during autumn is of great significance to seasonal climate prediction.

The variability of the Eurasian snow cover in each autumn month has distinct features and generates different influences on the atmosphere (Furtado et al., 2016; Han & Sun, 2018; Ye & Wu, 2017). Among them, the November snow cover anomaly has attracted growing interest due to its pronounced influences on atmospheric circulations and regional climate variabilities in the following seasons (Ao & Sun, 2016; Henderson et al., 2018; Li et al., 2020; Yang & Fan, 2021; Ye, 2019). In particular, a zonal dipole structure of the November snow cover anomaly, with two opposite-sign centers over the west and east sides of mid-latitudes of Eurasia, could strongly affect the intensity of the polar vortex in the stratosphere by regulating the upward propagation of the wave activity flux (Cohen et al., 2007). The signal of the polar vortex variability could transport downward to the lower troposphere in the following winter and lead to the persistent same signed anomalies in the Arctic Oscillation (AO) and North Atlantic Oscillation (NAO) and a widespread climate anomaly over northern Eurasia (Gastineau et al., 2017; Han & Sun, 2018; Santolaria-Otín et al., 2020; Wegmann et al., 2020). Additionally, the snow cover anomalies over the west and east centers can independently affect the winter climate over East Asia. For example, Ao and Sun (2016) found that there is a close connection between November snow cover over eastern Europe and winter precipitation over northern East Asia. Han and Sun (2021) suggested that the November snow cover over northeast Asia can affect the variability of south China precipitation in January through the troposphere–stratosphere coupling process. Given such profound climatic implications, it is important to understand whether the dipole pattern is the intrinsic mode of the Eurasian November snow cover variability and what factors account for the formation of this mode. However, these issues have received little attention from previous studies.

In theory, the snow cover anomaly is directly controlled by the variabilities in surface air temperature and snowfall. A number of studies have shown that there are multiple atmospheric teleconnection patterns prevailing over Eurasia that can significantly affect large-scale atmospheric circulations and therefore induce temperature and precipitation anomalies (Barnston & Livezey, 1987; Chen et al., 2016; Liu et al., 2014; Song et al., 2022; Wallace & Gutzler, 1981). This implies that the anomalous atmospheric circulations associated with the teleconnection patterns may be the vital influencing factors of the snow cover anomaly. For instance, several previous studies have demonstrated that the thermal advection induced by the NAO, Scandinavian pattern (SCAND), and Eastern Atlantic pattern (EA) could well explain the variability in European snow cover in winter (Clark et al., 1999; Henderson & Leathers, 2010; Kim et al., 2013; Seager et al., 2010). Recently, Zhang, Wang, Zhao, et al. (2021) indicated that the first two leading modes of Eurasian snow cover anomalies during spring are mainly shaped by the AO, Polar–Eurasian pattern (POL), West Pacific pattern (WP), and East Atlantic–Western Russia pattern (EAWR). To date, the influences of teleconnections on autumn snow cover have not been well understood compared to those in winter and spring. Although Gastineau et al. (2017) reported a close connection of November snow cover over eastern Siberia with SCAND, it remains unclear whether there is any other teleconnection that has the capacity to affect the November dipole snow cover variability and to what extent these teleconnections can explain the anomaly of snow cover.

Furthermore, previous studies found that the anomalies of sea surface temperature (SST) and sea ice concentration are the considerable drivers of the Eurasian snow cover variability. For example, Sun et al. (2019) suggested that a basin-wide warming of North Atlantic SST contributed to the decadal shift of Eurasian winter snow mass in the early 2000s. Zhang, Wang, Zhao, et al. (2021) indicated that a horseshoe-like structure of the North Atlantic SST anomalies exert a remarkable effect on the interannual variability of Eurasian snow cover during spring. In addition, the sea ice variations over the Barents–Kara Sea can modulate the Eurasian snow cover variability during winter and spring (Xu et al., 2019; Zhang, Wang, Zhao, et al., 2021). However, it is still unknown whether these oceanic forcings have potential influences on the dipole mode of the snow cover anomaly during autumn.

Therefore, the purpose of this study is to reveal the potential drivers of the dipole pattern of Eurasian November snow cover variability by specifically considering the impacts of atmospheric teleconnection patterns and the anomalies of SST and Arctic sea ice. The remainder of this paper is organized as follows. The datasets and methods used in this study are described in Section 2. In Sections 3 and 4, we investigated the features as well as the potential influencing factors and the associated physical processes of the dipole snow cover variability over Eurasia during late autumn. Finally, a summary and discussion are given in Section 5.

2. Data and Methods

The snow cover data used in this study is Northern Hemisphere EASE-Grid 2.0 Weekly Snow Cover and Sea Ice Extent, Version 4, which is available from 1966 to present and can be downloaded from the National Snow and Ice Data Center (NSIDC, Brodzik & Armstrong, 2013). The raw data are stored as flat binary files in arrays of 720 columns by 720 rows, with values of 0 or 1 indicating the coverage fraction of snow less or larger than 50% in each cell. To conveniently represent the variability of snow cover, we calculated the monthly snow cover fraction (SCF), which is expressed as the ratio of the numbers of days in a month for which snow was present to the total number of days in that month. In addition, the monthly snow cover extent data provided by the Japan Aerospace Exploration Agency Satellite Monitoring for Environmental Studies (JASMES, Hori et al., 2017) was also employed to corroborate the results obtained from the NSIDC data. The JASMES data has a high spatial resolution of 5 km × 5 km, and covers the period from 1978 to 2019, but lacks the data in November of 1980 and 1994. To facilitate the analysis, we converted the snow cover data of both the NSIDC and JASMES to a regular 1° × 1° longitude-latitude grid using the linear interpolation method.

The surface air temperature (SAT) data was derived from the Climate Research Unit, University of East Anglia (CRU TS v4.03), which covers the period from 1901 to the present and has a spatial resolution of 0.5° × 0.5° (Harris et al., 2020). The monthly snowfall data with a horizontal resolution of 1.25° × 1.25° spanning 1958 to the present is from the Japanese 55-year Reanalysis (JRA-55, Kobayashi et al., 2015). The monthly mean SST data was from the National Oceanic and Atmospheric Administration (NOAA) Extended Reconstructed Sea Surface Temperature (ERSST) v5 data set, which is on a 2° × 2° grid and covers the period since 1854 (Huang et al., 2017). Sea ice concentration was extracted from the Hadley Centre Sea Ice and Sea Surface Temperature data set (HadISST1), which has a horizontal resolution of 1° × 1° and the temporal coverage from 1870 to the present (Rayner et al., 2003). Other monthly atmospheric variables, such as geopotential height, sea level pressure, horizontal wind, total cloud cover, perceptible water, air temperature, sensible and latent heat fluxes, downward longwave and shortwave radiation fluxes, were extracted from the National Centers for Environmental Prediction-National Center for Atmospheric Research (NCEP-NCAR) Reanalysis 1 product (Kalnay et al., 1996). The NCEP-NCAR atmospheric data have a horizontal resolution of 2.5° × 2.5°, except for the total cloud cover and energy fluxes, which are on the T62 Gaussian grid. The same variables from the European Centre for Medium-Range Weather Forecasts (ECMWF) Reanalysis v5 (ERA5, Hersbach et al., 2019) were also used in this study to corroborate the results.

The teleconnection pattern indices, including the AO, NAO, EA, EAWR, SCAND, POL, and WP were obtained from the NOAA Climate Prediction Center. In addition, the index of the Eurasian pattern (EU) was also used in the present study, which was calculated following the definition of Wallace and Gutzler (1981):

$$\mathrm{EU} = -\frac{1}{4}\mathrm{Z}^*(55°\mathrm{N}, 20°\mathrm{E}) + \frac{1}{2}\mathrm{Z}^*(55°\mathrm{N}, 75°\mathrm{E}) - \frac{1}{4}\mathrm{Z}^*(40°\mathrm{N}, 145°\mathrm{E}) \tag{1}$$

where Z* denotes the normalized monthly mean 500 hPa geopotential height anomalies at the corresponding locations. These teleconnections were chosen because they all exert significant impacts on the Eurasian climate (Barnston & Livezey, 1987; Liu et al., 2014; Thompson & Wallace, 1998; Wallace & Gutzler, 1981).

To diagnose the impacts of atmospheric circulations on SAT variability, we calculated the horizontal thermal advection (T_{adv}) using the NCEP-NCAR reanalysis data according to the formula in Holton (1992):

$$T_{\mathrm{adv}} = -u\frac{\partial T}{r\cos\varphi\partial\lambda} - v\frac{\partial T}{r\partial\varphi} \tag{2}$$

where λ and φ are the longitude and latitude, respectively, and r, T, u, and v denote the radius of Earth, surface temperature, and surface zonal and meridional winds, respectively.

The wave activity flux (WAF) proposed by Takaya and Nakamura (1997, 2001) was used to diagnose the propagation of the wave train. The horizontal components of WAF were defined as follows:

$$\mathrm{WAF} = \frac{p\cos\varphi}{2|\mathbf{U}|}\begin{Bmatrix} \frac{U}{\alpha^2\cos^2\varphi}\left[\left(\frac{\partial\psi'}{\partial\lambda}\right)^2 - \psi'\frac{\partial^2\psi'}{\partial\lambda^2}\right] + \frac{V}{\alpha^2\cos\varphi}\left[\frac{\partial\psi'}{\partial\lambda}\frac{\partial\psi'}{\partial\varphi} - \psi'\frac{\partial^2\psi'}{\partial\lambda\partial\varphi}\right] \\ \frac{U}{\alpha^2\cos\varphi}\left[\frac{\partial\psi'}{\partial\lambda}\frac{\partial\psi'}{\partial\varphi} - \psi'\frac{\partial^2\psi'}{\partial\lambda\partial\varphi}\right] + \frac{V}{\alpha^2}\left[\left(\frac{\partial\psi'}{\partial\varphi}\right)^2 - \psi'\frac{\partial^2\psi'}{\partial\varphi^2}\right] \end{Bmatrix} \tag{3}$$

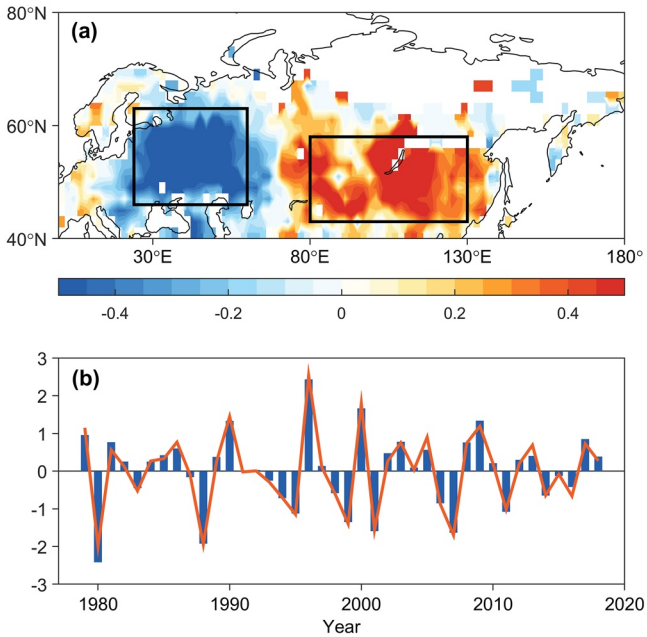

Figure 1. The first EOF mode of November Eurasian snow cover variability during 1979–2018. (a) The spatial pattern, (b) PC1 (blue bars) and SCVI (red curve). The black boxes in (a) denote the regions where the snow cover was used to construct the SCVI.

where |**U**| represents the climatological magnitude of winds, α is the mean radius of the earth, p denotes the pressure scaled by 1,000 hPa, φ and λ are latitude and longitude, U and V denote the climatological zonal and meridional wind, respectively, and ψ' is the perturbed geostrophic streamfunction.

The present study mainly focuses on the interannual variability, therefore, all of the variables were subjected to a 9-year Lanczos high-pass filter (Duchon, 1979) before analysis to avoid the contamination of the signals of decadal variations and long-term trend. We conducted empirical orthogonal function (EOF) analysis to extract the leading modes of the variability in Eurasian snow cover. In addition, linear regression, correlation and partial correlation analyses were used to examine the statistical connections between variables. The significance level of the analyses was estimated using the standard two-tailed Student's t test method.

3. The Dipole Mode of the November Snow Cover Variability

Figure 1 shows the results of the EOF analysis on the November SCF variability over northern Eurasia (0°–180°, 40°N–80°N) during 1979–2018. The first EOF mode (EOF1) accounts for 19% of the total variance and clearly separates from the remaining modes according to the criterion of North et al. (1982). The spatial pattern of EOF1 features a prominent zonal dipole structure over the mid-latitudes of Eurasia, with one center over eastern Europe and the other center, with the opposite sign, over the region to the northeast of Lake Balkhash and the vicinity of Lake Baikal (Figure 1a). The locations of the two active centers are generally consistent with the key regions found by previous studies (Gastineau et al., 2017; Han & Sun, 2018; Santolaria-Otín et al., 2020; Wegmann et al., 2020). These studies indicated that the snow cover over these regions have significant effects on the large-scale atmospheric circulations and climate in the following seasons.

To further interpret the physical significance of the EOF1 mode, we constructed a snow cover variability index (SCVI), which is computed as the normalized difference between the area-weighted regional mean SCF over the east (80°−130°E, 43°–58°N) and west (25°−60°E, 47°–62°N) centers of the loading of EOF 1 (illustrated by the black boxes in Figure 1a). As shown in Figure 1b, the SCVI varies synchronously with the principal component (PC1), with a correlation coefficient between them as high as 0.99 ($P < 0.001$) during the research period. This indicates that the positive polarity of PC1 denotes above-normal snow cover over the eastern center but less snow cover over the west. The opposite pattern would appear when PC1 is in the negative phase. In addition, we have further performed an EOF analysis on the JASMES snow cover data during 1979–2018 except for the 1980 and 1994 owing to the missing data. As shown in Figure S1a in Supporting Information S1, the second EOF mode of JASMES also features an apparent zonal dipole pattern over the mid-latitudes of Eurasia, which is generally consistent with that of EOF1 from the NSIDC data (Figure 1a). Moreover, the PC of the EOF2 derived from the JASMES data matches well with that of EOF1 from the NSIDC data, with the correlation coefficient as high as 0.83, significant at 99.9% confidence level (Figure S1b in Supporting Information S1). These consistencies regarding the spatial pattern and the temporal evolution between the results obtained from the JASMES and NSIDC confirm that our result is not sensitive to the selection of data, and further suggests that the zonal dipole pattern is the intrinsic mode of November snow cover variability over Eurasia. In the following sections, we used the PC1 of the snow cover variability from NSIDC as the index of the dipole mode of snow cover variability for further analyses.

4. Causes for the Formation of the Dipole Mode

4.1. The Dipole Mode-Related Atmospheric Circulations

The snow cover anomaly is the product of the variabilities in surface air temperature and precipitation, which are in turn profoundly modulated by atmospheric circulations. Figure 2 exhibits the anomalous atmospheric

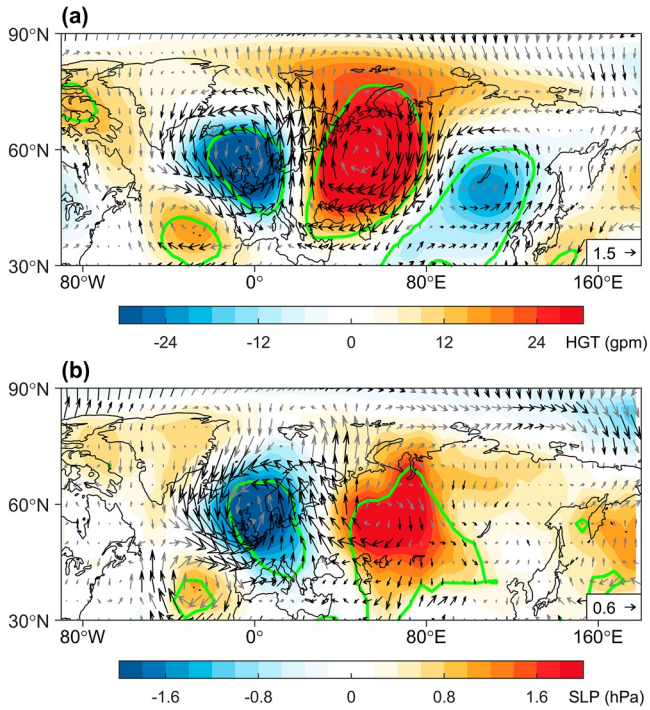

Figure 2. Anomalies of atmospheric circulations obtained by regression onto PC1 during 1979–2018. (a) 500 hPa geopotential height (shading) and horizontal wind (vectors; m s^{-1}), (b) sea level pressure (shading) and 10 m wind (vectors; m s^{-1}). Black vectors and green lines denote the wind, geopotential height and sea level pressure anomalies significant at the 95% confidence level, respectively.

circulations at the surface and mid-troposphere obtained by regression against PC1. It is obvious that a prominent wave train-type anomalous circulation appears at 500 hPa and propagates from the North Atlantic to the Northwest Pacific across the Eurasian continent (Figure 2a). Corresponding to the positive phase of the PC1, the negative and positive snow cover anomalies over the western and eastern key regions (Figure 1a) are controlled by the anomalous anticyclonic and cyclonic circulations centered over the west Siberia and Lake Baikal, respectively (Figure 2a). The anomalous circulations in the lower troposphere bear a close resemblance to those at the mid-level, although the cyclonic circulation around Lake Baikal is relatively weak at the surface (Figure 2b), indicating a quasi-barotropic structure. Similar results were found when the ERA5 data set was used (Figure S2 in Supporting Information S1).

On the west flank of the anticyclonic circulation over the west Siberia, the anomalous southerly wind prevails over eastern Europe (Figure 2b), which leads to the negative anomalies of snow cover over there (Figure 1a) by bringing warmer air from the lower latitudes. The positive anomalies of snow cover to the northeast of Lake Balkhash could be attributed to the anomalous northerly wind that is conducive to the reduction of air temperature. In addition, the positive anomalies of snow cover in the vicinity of Lake Baikal may result from anomalous cyclonic circulation, which allows more precipitation and less solar radiation by intensifying upward air motion. These analyses suggest that the atmospheric circulations play a crucial role in the formation of snow cover anomalies related to the dipole mode. A question naturally raised: what factors drive these anomalous atmospheric circulations? Previous studies have indicated that the large-scale atmospheric teleconnection patterns are the important factors driving the changes in atmospheric circulations over Eurasia (Chen et al., 2016; Song et al., 2022; Zhang, Wang, Zhao, et al., 2021). Therefore, in the next section, we investigated the potential influences of atmospheric teleconnections on the dipole mode of snow cover variability.

4.2. Contributions of Atmospheric Teleconnections

Several atmospheric teleconnections prevail over Eurasia. In order to identify the key teleconnection patterns that have a potential influence on the snow cover variability, we employed a correlation analysis between the teleconnection indices and PC1. As shown in Table 1, PC1 has a significantly positive correlation with EA and SCAND, with correlation coefficients of 0.45 and 0.4, respectively. In addition, PC1 is negatively correlated with EAWR, with a correlation coefficient as high as −0.48, which is significant at the 1% level. The results indicate that the atmospheric circulations related to these teleconnection patterns can exert critical effects on the formation of the dipole mode of Eurasian November snow cover variability.

Table 1
The Correlation Coefficients of PC1 of Eurasian November Snow Cover Variability With Various Atmospheric Teleconnection Indices

Teleconnection indices	Correlation coefficients
AO	0.04
EA	**0.45***
EAWR	**−0.48***
EU	0.13
NAO	−0.11
POL	0.22
SCAND	**0.40***
WP	0.06

Note. The bold values with asterisks denote that the correlation coefficients are significant at the 95% confidence level.

Figure 3 illustrates the atmospheric circulation anomalies and wave structure associated with EA, EAWR, and SCAND, respectively. As indicated by the wave activity flux, the anomalous circulations related to the teleconnections exhibit the clear wave train pattern propagating eastward from the North Atlantic to the Eurasia (Figures 3a, 3d and 3g). The anomalous circulations and the wave train structure related to one teleconnection pattern are different from that related to others, implying that the atmospheric circulations associated with the teleconnections could exert independent influences on the snow cover variability. Corresponding to the positive phase of EA, there is an anomalous ridge stretching from the coast of the Kara Sea to the Balkan

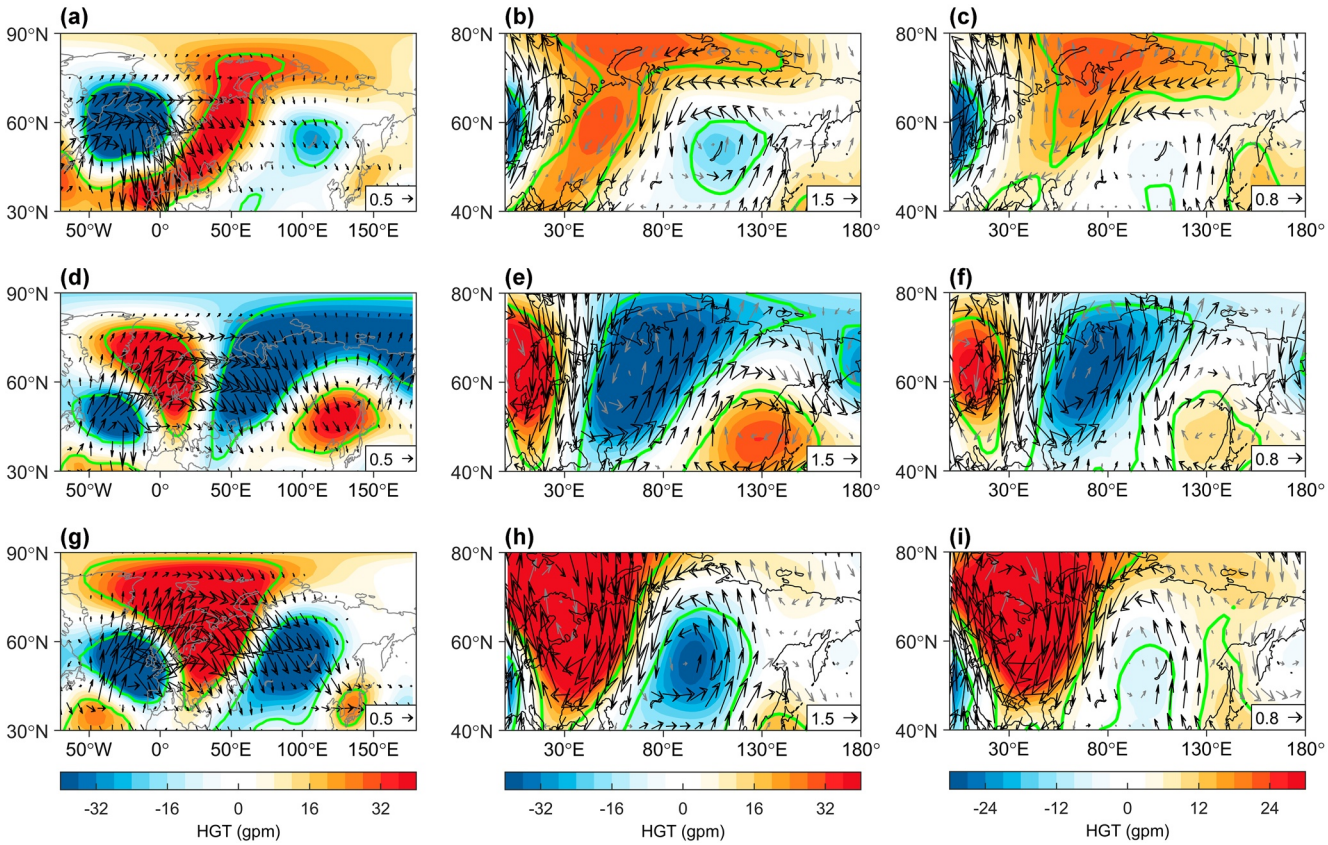

Figure 3. Anomalies of geopotential height (shading) at 200 hPa (left panel), 500 hPa (middle panel) and 850 hPa (right panel) obtained by regression against EA (a–c), EAWR (d–f), and SCAND (g–i). The vectors in left panel denote the wave activity flux ($m^2\ s^{-2}$) associated with the corresponding teleconnections. The vectors in middle and right panels indicate the horizontal wind anomalies ($m\ s^{-1}$) obtained by regression onto the relevant teleconnection indices. The black vectors and the areas circled by green solid lines denote the anomalies of wind and geopotential height significant at the 95% confidence level, respectively.

Peninsula and a cyclonic circulation around Lake Baikal at 500 hPa (Figure 3b). The circulation anomalies pattern at 850 hPa are generally consistent with those at 500 hPa, except for the relatively weaker cyclonic circulation around Lake Baikal (Figure 3c). The anomalous southwesterly winds on the west side of the ridge bring abundant moisture from the North Atlantic to eastern Europe, leading to above-normal cloud cover and precipitable water there (Figures 4a and 4b). As a result, the downward shortwave radiation decreased, while the downward longwave radiation significantly increased over eastern Europe (Figures 4c and 4d). The pronounced positive SAT anomaly occurred in eastern Europe (Figure 4g), which could be mainly attributed to the increased downward longwave radiation (Figure 4d) because the anomalies of thermal advection over this region are not significant, and thus may have little contribution to the increase of SAT over there (Figure 4e). Due to the warmer atmosphere and the divergence of the anomalous ridge, significantly reduced snowfall is seen over eastern Europe (Figure 4f), despite the excessive moisture there. Therefore, jointly influenced by the warmer SAT and lesser snowfall, the snow cover has significantly reduced over eastern Europe (Figure 4h). In addition, over the east center of the dipole mode, the anomalous cyclonic circulation results in more cloud cover and snowfall to the south of Lake Baikal (Figures 4a and 4f), which leads to decreased incoming solar radiation and hence a colder temperature (Figures 4c and 4g). As a result, the positive anomalies of snow cover were observed to south of Lake Baikal (Figure 4h).

In response to the positive phase of EAWR, a strong anomalous cyclonic circulation appears in west Siberia and two anomalous anticyclonic circulations presents over the Scandinavian Peninsula and east of Lake Baikal, respectively (Figure 3e). This circulation pattern is robust in both the mid and lower troposphere, indicating a quasi-barotropic structure (Figures 3e and 3f). In accordance with the anomalous circulation, the anomalies of total cloud cover exhibit a tripole pattern, with two negative centers distributed on the west and east sides of Eurasia due to the controlling of the anticyclonic circulations and one positive center over western Siberia induced

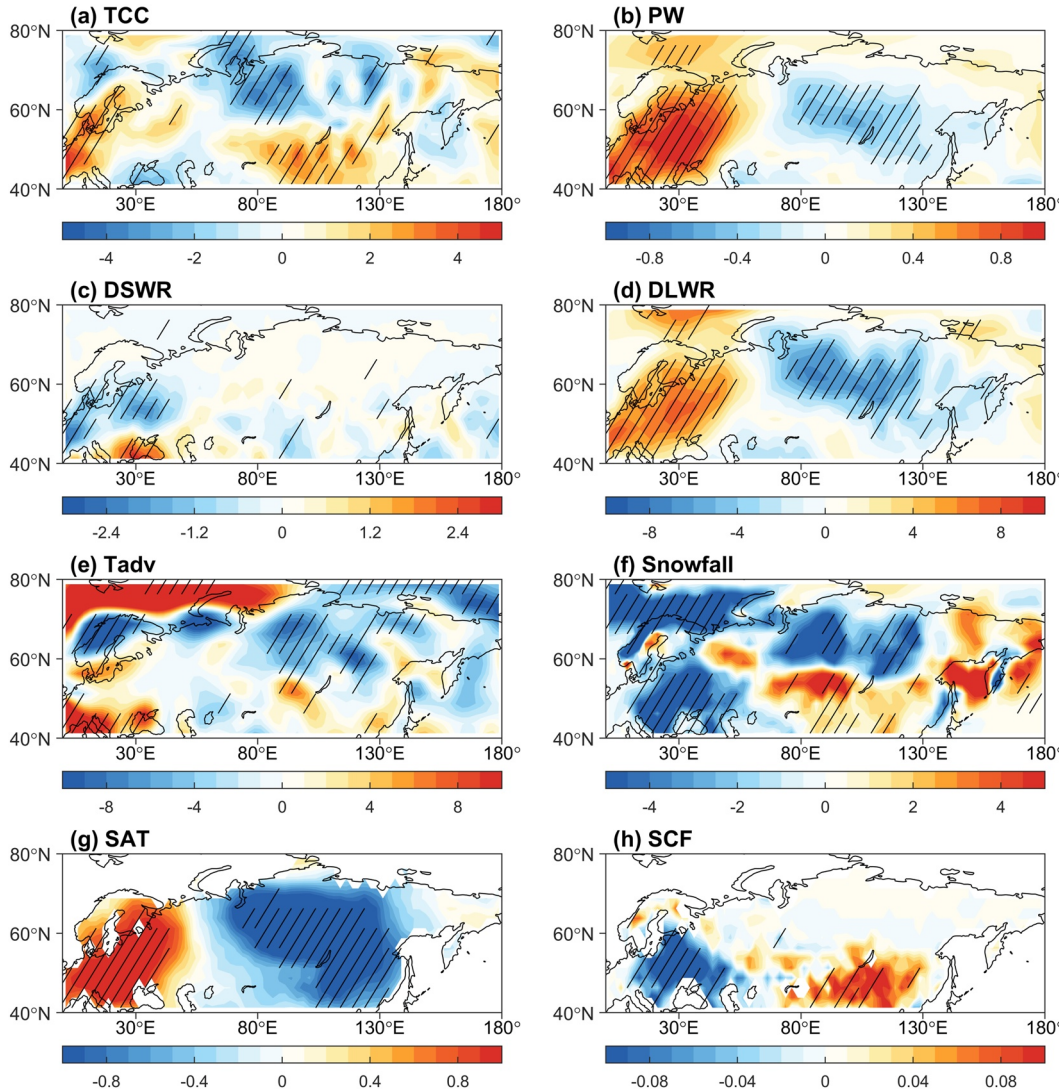

Figure 4. Anomalies of (a) total cloud cover (%), (b) precipitable water (kg m^{-2}), (c) downward shortwave radiation flux (W m^{-2}), (d) downward longwave radiation flux (W m^{-2}), (e) thermal advection (°C), (f) snowfall (mm), (g) surface air temperature (°C), and (h) snow cover fraction obtained by regression onto the index of EA. The hatched areas denote the anomalies of the variables significant at the 95% confidence level.

by the anomalous cyclone (Figure 5a). Accordingly, the downward solar radiation anomalies have also formed a tripole pattern that is consistent with those of total cloud cover but with the opposite signs (Figure 5c). Negative anomalies of precipitable water are seen over western Siberia and eastern Europe (Figure 5b), which could be attributed to the anomalous northerly winds on the west flank of the cyclone that bring cold air from the high latitudes and hence reduce the water-holding capacity of the atmosphere (Figures 3e and 3f). As a result, the downward longwave radiation and SAT significantly decreased over the same region (Figures 5d and 5g). In addition, significantly positive anomalies of snowfall are observed over eastern Europe and western Siberia (Figure 5f) due to the effect of the strong cyclonic circulation (Figure 3f). Therefore, in conjunction with the increased snowfall and decreased SAT, above-normal snow cover appears in eastern Europe and western Siberia (Figure 5h). Over Lake Baikal and its adjacent areas, the positive SAT anomalies can be seen as a consequence of the anomalous anticyclonic circulation (Figure 3f; Figure 5g). Such an anticyclone, on the one hand, acts to transport warmer air from lower latitudes to the region around Lake Baikal through anomalous southerly winds (Figure 3f; Figure 5e). On the other hand, the anticyclonic flow would further warm the air temperature by suppressing the upward motion that leads to a reduction in cloud cover and an increase in downward solar radiation (Figures 5a and 5c). Additionally, under the control of the anticyclonic circulation, negative anomalies of snowfall were observed

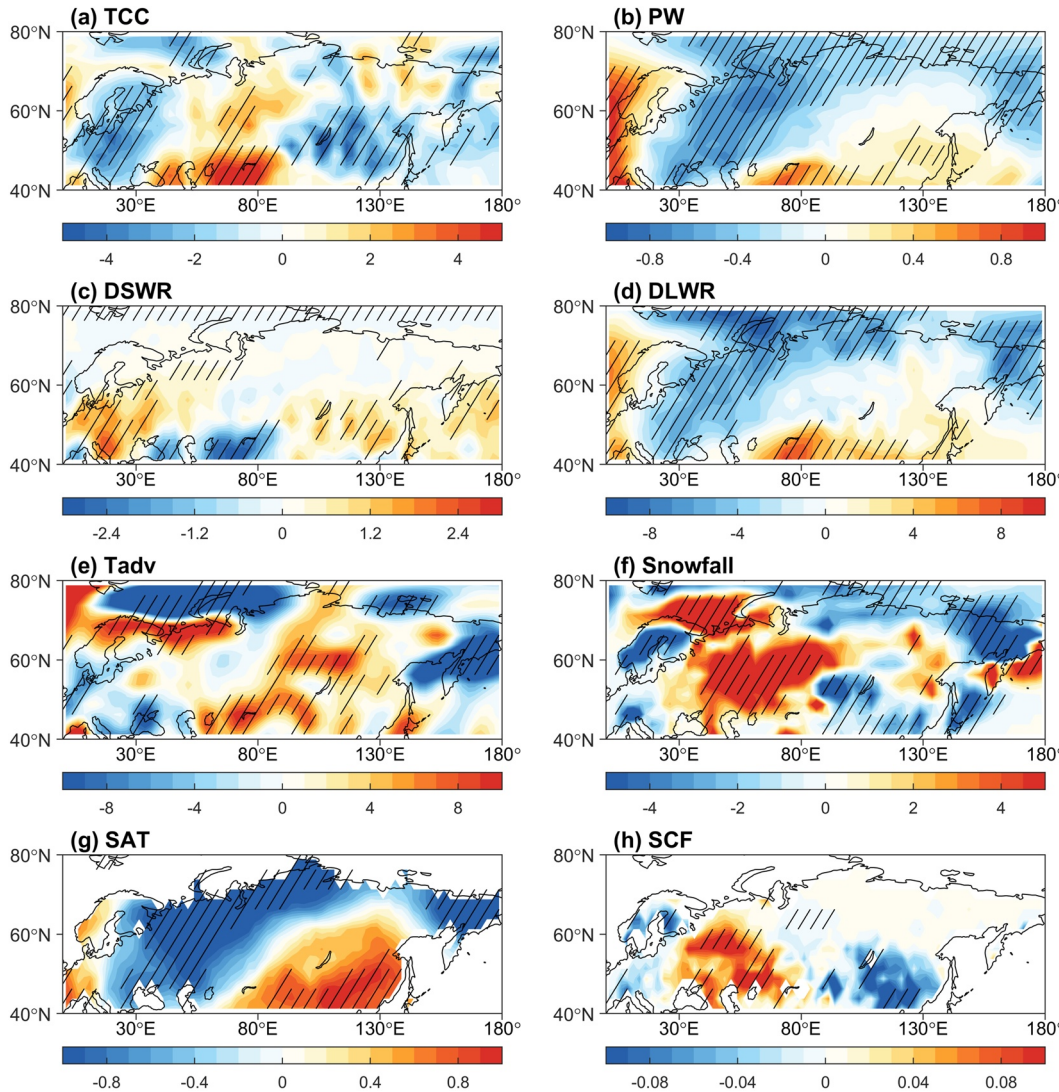

Figure 5. Same as Figure 4 but obtained by regression onto the EAWR index.

around Lake Baikal (Figure 5f). The joint effects of negative snowfall and positive SAT eventually lead to the reduced snow cover in the vicinity of Lake Baikal (Figure 5h).

For the positive phase of SCAND, a prominent anticyclonic circulation is seen over northern Scandinavia and eastern Europe in both the mid and lower troposphere, and an anomalous cyclonic circulation is observed over the region to the west of Lake Baikal (Figures 3h and 3i). The anomalous ridge over eastern Europe leads to a decrease in local cloud cover and snowfall by suppressing water vapor convergence (Figures 6a and 6f). The reduced cloud cover further causes positive downward solar radiation anomalies to the north of the Caspian Sea (Figure 6c). In addition, the anomalous northerly winds on the east flank of the anticyclone and the west flank of the cyclone jointly transport cold air from high latitudes southwestward to the Caspian Sea, which results in decreased precipitable water due to the lower water-holding capacity of colder air (Figures 3h and 3i; Figures 6b and 6e). As a result, reduced downward longwave radiation and SAT were observed over the corresponding region (Figures 6d and 6g). Therefore, the negative anomalies of snow cover over eastern Europe (Figure 6h) may be primarily contributed by the decreased snowfall (Figure 6f). Over the mid-latitudes of eastern Eurasia, the anomalous cyclonic circulation contributes to positive cloud cover and snowfall anomalies around Lake Balkhash (Figures 6a and 6f), which further leads to excessive snow cover (Figure 6h). In addition, the above normal snow cover around Lake Baikal could be mainly attributed to the decreased SAT, which in turn may result from the reduced downward longwave radiation (Figures 6d, 6g and 6h).

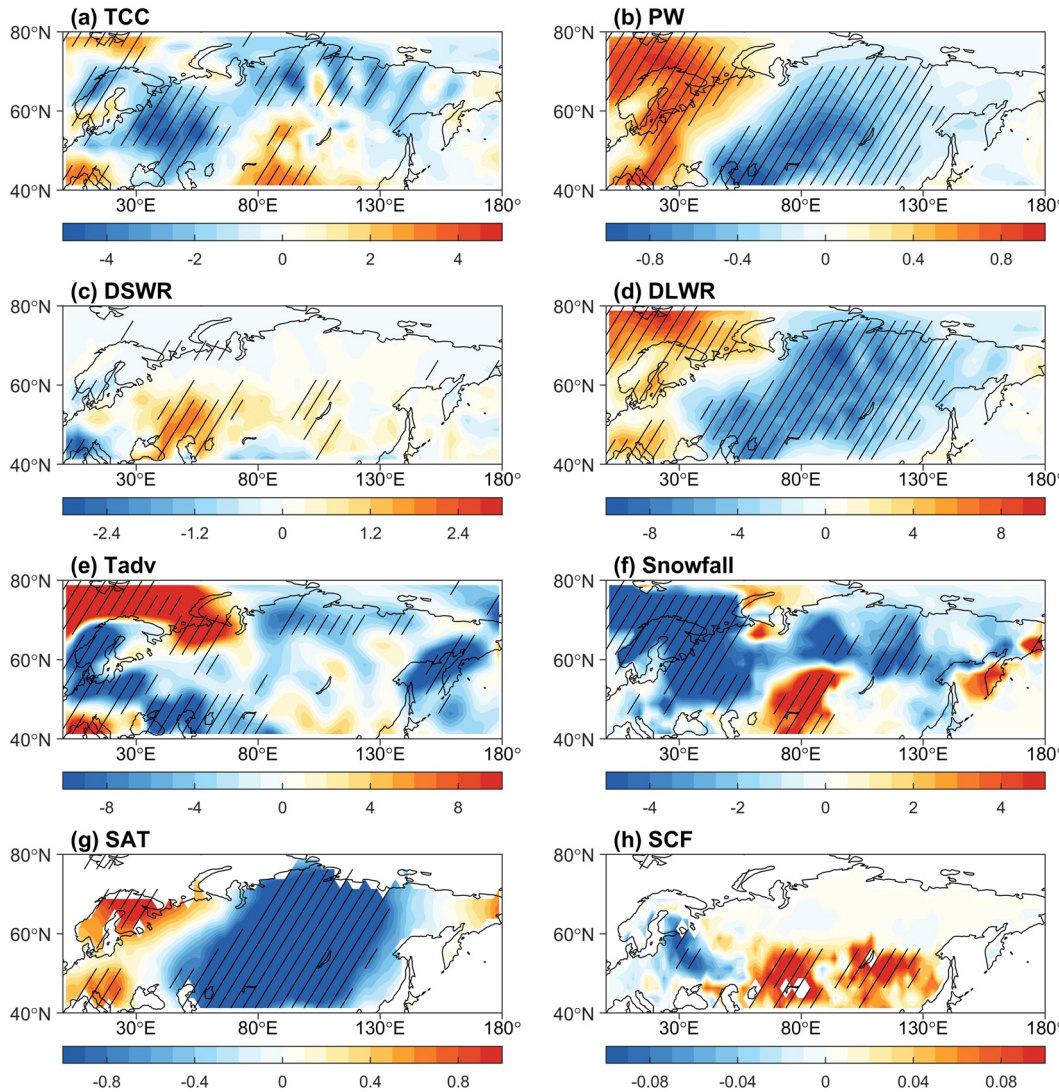

Figure 6. Same as Figure 4 but obtained by regression onto the index of SCAND.

4.3. Role of the SST Anomalies

It is apparent that the anomalous atmospheric circulations responsible for the dipole pattern of snow cover variability exhibit a clear wave train structure emanating from the North Atlantic (Figure 2a). This implies that the North Atlantic SST anomalies may play an important role in trigging this anomalous circulation and the resultant snow cover variability. To examine this hypothesis, we calculated the November global SST anomalies obtained by regression against the PC1. The significant SST anomalies are mainly located over the North Atlantic, supporting our conjecture (Figure S3 in Supporting Information S1). Zooming in on the North Atlantic (Figure 7a), there is an obvious dipole pattern of SST anomalies, with significantly positive anomalies over the central North Atlantic and negative anomalies over the region to the south of the Iceland. To further explore the impact of such SST anomalies, we defined a dipole SST anomalies index (SSTI) as the normalized difference between the area mean SST over the south (25–45°W, 30–43°N) and north (10–35°W, 49–60°N) anomalies centers (Figure 7a). As shown in Figure 7b, the SSTI has a close connection with the PC1, with the correlation coefficient between them of 0.53, significant at the 99.9% confidence level, suggesting the potential effect of the dipole SST anomalies on the Eurasian snow cover variation. In the following, we would investigate the physical process responsible for this SST-snow linkage.

The influences of the SST anomalies over the North Atlantic on the climate variability over Eurasia have been extensively explored by previous observational and modeling studies (Chen et al., 2016; Choi & Ahn, 2019; Sun et al., 2019; Wu et al., 2011; Zhang, Wang, Zhao, et al., 2021). They indicated that the North Atlantic SST

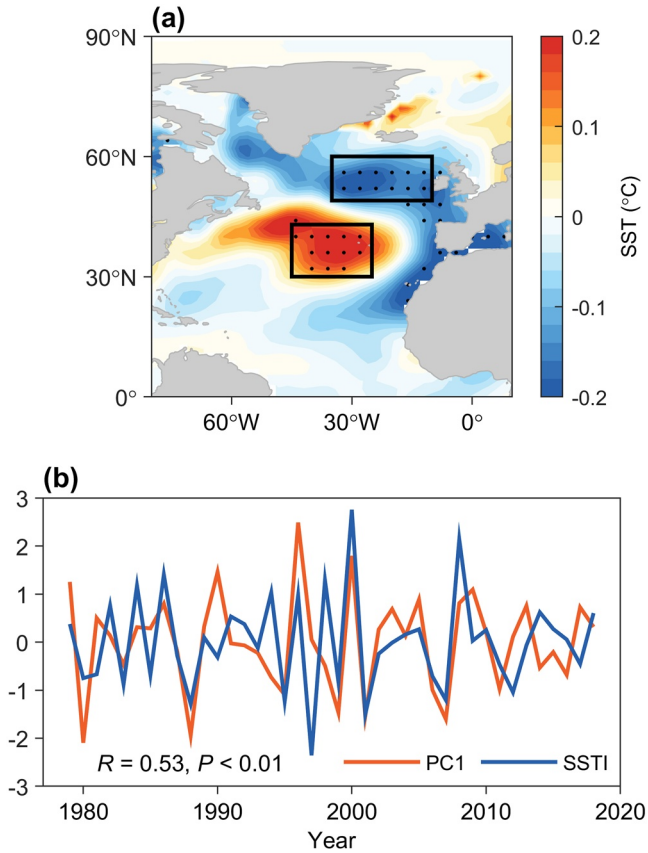

Figure 7. Anomalies of North Atlantic SST during November obtained by regression onto PC1 (a). (b) The timeseries of PC1 and SSTI. Stippling regions denote SST anomalies significant at the 95% confidence level. The black boxes in (a) denote the regions where the SST was used to construct the SSTI.

anomalies induced atmospheric perturbation at upper troposphere is the effective Rossby wave source, which could excite an eastward propagating atmospheric wave train over Eurasia (Chen et al., 2016, 2020; Watanabe, 2004). Here we show that in response to the positive phase of the SSTI, a prominent wave train stems from the central North Atlantic and propagates northeastward to the Ireland, and then turns eastward to the eastern Europe and Lake Baikal (Figure 8a). Corresponding to this wave train, a significantly anomalous anticyclonic circulation appears over the eastern Europe and an anomalous cyclonic circulation dominates the region around the Lake Baikal (Figure 8b). This anomalous circulation pattern can be seen at both the middle and lower troposphere, indicating a barotropic structure (Figures 8b and 8c). The anomalous anticyclone is conducive to the divergent circulation and the descending air motion that would contribute to the decrease in precipitation and increase in SAT through reducing the cloud coverage and enhancing the incoming solar radiation at the surface. As a result, the negative anomalies of snow cover formed over the eastern Europe (Figure 8c). In the vicinity of the Lake Baikal, the significantly positive anomalies of snow cover could be attributed to the anomalous cyclone (Figures 8b and 8c), which would induce increased precipitation and decreased SAT by strengthening the moisture convergence and reducing the incoming solar radiation. The pattern of snow cover anomalies associated with the SSTI (Figure 8c) closely resembles that of the EOF1 mode (Figure 1a), confirming the considerable effect of the North Atlantic SST anomalies on the formation of the dipole mode of the Eurasian snow cover variability.

Previous studies indicated that the atmospheric teleconnection patterns investigated in the above section may be modulated by the North Atlantic SST anomalies (Gao et al., 2017; Liu et al., 2014). It raises a doubt that whether the anomalous atmospheric circulations induced by the dipole SST anomalies are independent of those associated with these teleconnection patterns. Here, we found that the SSTI has negligible connections with EA, EAWR, and SCAND, with the correlation coefficients of 0.27, −0.22, and 0.29, none of them reach the 95% confidence level. It suggests that the dipole SST anomalies have little contribution to the formation of these teleconnection patterns. In addition, the partial correlation analyses denote that the correlation between SSTI and PC1 is still significant after removing the effects of the teleconnections, as is the correlation between teleconnection indices and PC1 after removing the signal of SSTI (Table S1 in Supporting Information S1). These results imply that the dipole pattern of the North Atlantic SST anomalies and the atmospheric circulations related to the teleconnection patterns can exert the independent influences on the Eurasian snow cover variability.

4.4. Influence of Arctic Sea Ice Variations

The Arctic sea ice variations have been recognized as an important driver of the Eurasian climate variabilities in recent years (Bailey et al., 2021; Gao et al., 2015; Sun et al., 2022; Xu et al., 2019). In this section, we would examine whether the Arctic sea ice variations have a contribution to the formation of the dipole snow cover variability. For this purpose, we presented the distribution of the correlation coefficients between the PC1 and the simultaneous Arctic sea ice variations in Figure 9a, which shows that the significantly negative correlations are mainly located in the Barents Sea. To further confirm this relationship, we defined the Arctic sea ice index (SICI) as the normalized area mean sea ice concentration over the Barents Sea (20°−62°E, 75°–78°N) according to Figure 9a. The correlation coefficient between the SICI and the PC1 is as high as −0.51, exceeding the 99% confidence level. It denotes that the sea ice over the Barents Sea could account for about 26% of the snow cover variability related to the dipole mode.

To further understand the physical processes responsible for the influence of the Barents sea ice variations on the Eurasian snow cover variability, we investigated the anomalies of the atmospheric dynamic and thermodynamic

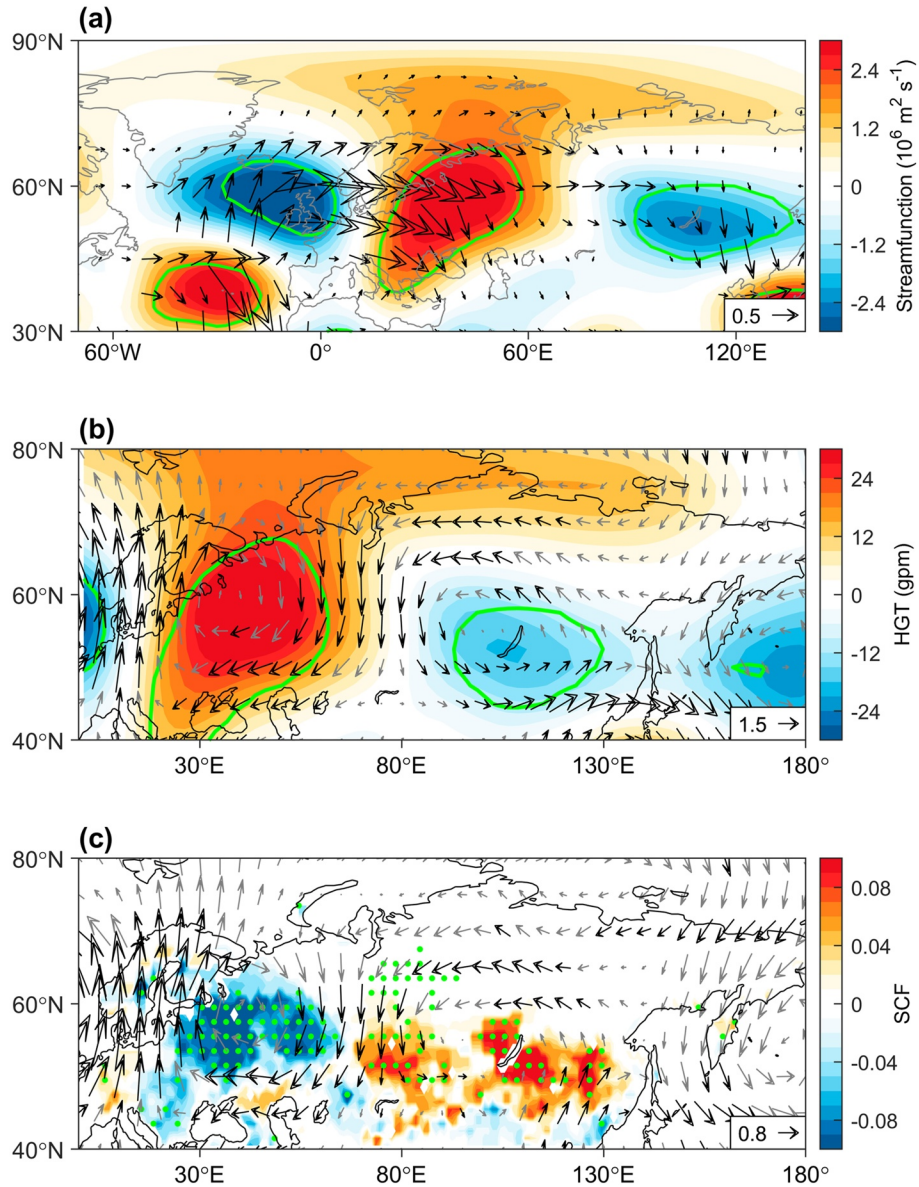

Figure 8. Anomalies of (a) streamfunction (shading) and wave activity flux (vectors; $m^2\ s^{-2}$) at 300 hPa, (b) geopotential height (shading) and horizontal wind (vectors; m s^{-1}) at 500 hPa, (c) horizontal wind (vectors; m s^{-1}) at 850 hPa and snow cover fraction (shading) obtained by regression against the SSTI. The black vectors in (b and c), the areas circled by green solid lines, and the dotted areas denote the anomalies significant at the 95% confidence level. The wave activity flux values less than 0.01 $m^2\ s^{-2}$ are not shown.

conditions related to the sea ice variations obtained by regression against the sign-reversed SICI. The decline of the sea ice is expected to cause more solar radiation to be absorbed by the ocean due to the reduced surface albedo, and enhance the heat exchange between the ocean and atmosphere (Chen et al., 2021; Dai et al., 2019). Here, we showed that, in response to the reduced sea ice over the Barents Sea, the turbulent heat flux (sum of the latent and sensible heat fluxes) from ocean to atmosphere has significantly strengthened over the corresponding region (Figure 10a), which further warms the overlying atmosphere (Figure 10b). The warming in the Arctic region would reduce the meridional temperature gradient between the mid and high latitudes, and thereby lead to the weakened westerly over the mid-latitudes of Eurasia according to the thermal wind relationship (Figure 10c). As suggested by previous studies, the deceleration of the westerly over the mid-latitudes would lead to the weakened synoptic-scale eddy activity that are accompanied by the positive geopotential height tendency to its north and the negative geopotential height tendency to its south (Cai et al., 2007; Chen et al., 2021; Lau, 1988). As a

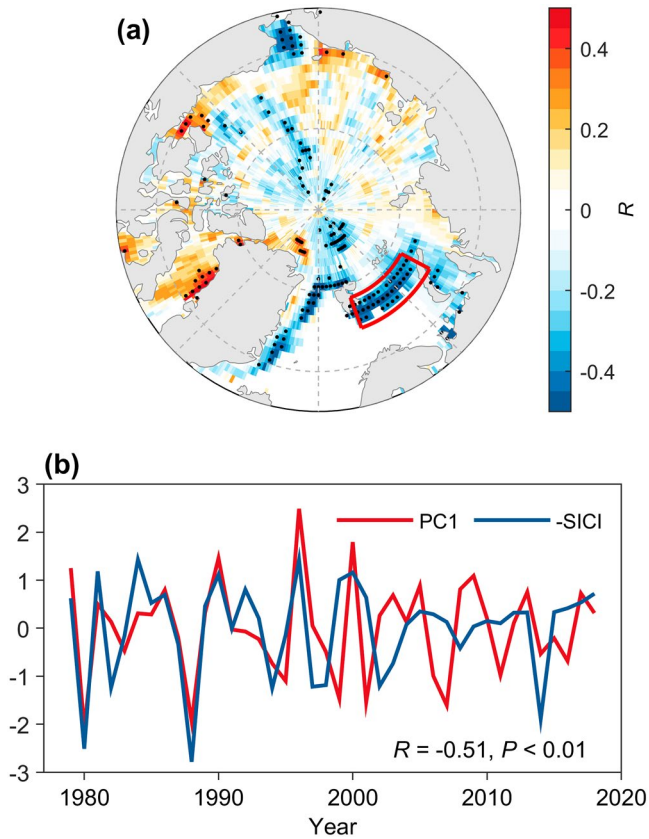

Figure 9. Correlation coefficients (*R*) between November sea ice concentration variation and PC1 (a). (b) The timeseries of PC1 and the sign-reversed SICI. Stippling regions in (a) denote *R* significant at the 95% confidence level. The red box in (a) denotes the region where the sea ice concentration was used to construct the SICI.

result, the significantly positive anomalies of the geopotential height appear over the northern west Siberia and the negative geopotential height anomalies occur to the southeast of the Lake Baikal (Figure 10d). This circulation anomalies pattern is also seen at the lower troposphere (Figure 10e), denoting a barotropic structure. On the southwest flank of the anomalous anticyclone, the anomalous southeast flow would transport warmer air from the lower latitudes (Figure 10e), which facilitates the snow ablation and hence leads to the negative anomalies of snow cover over Eastern Europe (Figure 10f). The positive anomalies of snow cover over the region between the Lake Balkhash and Lake Baikal may result from the anomalous northerly on the east side of the anticyclone that induced the cold advection favors the accumulation of snow cover (Figures 10e and 10f). In addition, the excessive snow cover to the southeast of Lake Baikal may be attributed to the anomalous cyclonic circulation (Figures 10e and 10f), which could lead to more precipitation by enhancing upward motion. Consequently, a zonal dipole pattern of snow cover anomalies presents over the mid-latitudes of Eurasia, confirming the important impact of the Barents sea ice variability.

4.5. Synergetic Effect of the Factors

The above analyses have verified the individual influence of the teleconnection patterns, North Atlantic SST anomalies and the Barents sea ice variations on the formation of the dipole mode of the Eurasian snow cover variability. In fact, the influences of these factors usually occurred concurrently. This implies that the anomalous atmospheric circulation related to one factor would be reinforced or counteracted by the superposition of those associated with another factor with the same or opposite signs, respectively. Therefore, in the following, we further investigated the synergetic effects of these influencing factors. For this purpose, we have constructed a composite index (CI) to represent the combined variations of these indices. The CI is defined as:

$$\mathrm{CI} = 0.29 \times \mathrm{EA} - 0.33 \times \mathrm{EAWR} + 0.31 \times \mathrm{SCAND} + 0.25 \times \mathrm{SSTI} - 0.25 \times \mathrm{SICI}$$

where the numbers multiplied by each index are the weighting coefficients, which are the corresponding regression coefficients obtained by the multiple linear regression of the indices onto PC1. As shown in Figure 11a, the CI has a significantly positive relationship with PC1, with a correlation coefficient as high as 0.81, which is much higher than that of PC1 with the individual index. This level of correlation means that the factors identified in this study could jointly account for about 66% of the interannual variability of the Eurasian snow cover related to the dipole mode.

To further examine the synergetic effect of these factors on the snow cover variability, the anomalous atmospheric dynamic and thermodynamic processes were analyzed through regression against the CI. Following the positive phase of CI, there is an obvious wave train propagating from the western Europe to the northeast Asia, with prominent anticyclonic and cyclonic circulations over eastern Europe and the vicinity of Lake Baikal, respectively (Figure 11b). The higher SAT over eastern Europe may mainly result from the anomalous southerly wind on the west flank of the anomalous anticyclone that could lead to the positive anomalies of the downward longwave radiation by increasing the atmospheric moisture content (Figures 11b, 11d and 11f). The decreased SAT around the Lake Baikal is jointly induced by the reduced downward shortwave and longwave radiation and the cold advection, which could be further attributed to the anomalous northerly wind and the convergent circulation associated with the anomalous cyclone (Figures 11b–11f). In contrast, the snowfall has significantly decreased over the eastern Europe and increased over the vicinity of Lake Baikal due to the controlling of the anomalous anticyclonic and cyclonic circulations, respectively (Figures 11b and 11g). Correspondingly, contributed by the combined effect of the variabilities of SAT and snowfall, a zonal dipole structure of snow cover anomalies is seen over the mid-latitudes of Eurasia (Figure 11h). These anomalies associated with the CI are generally consistent

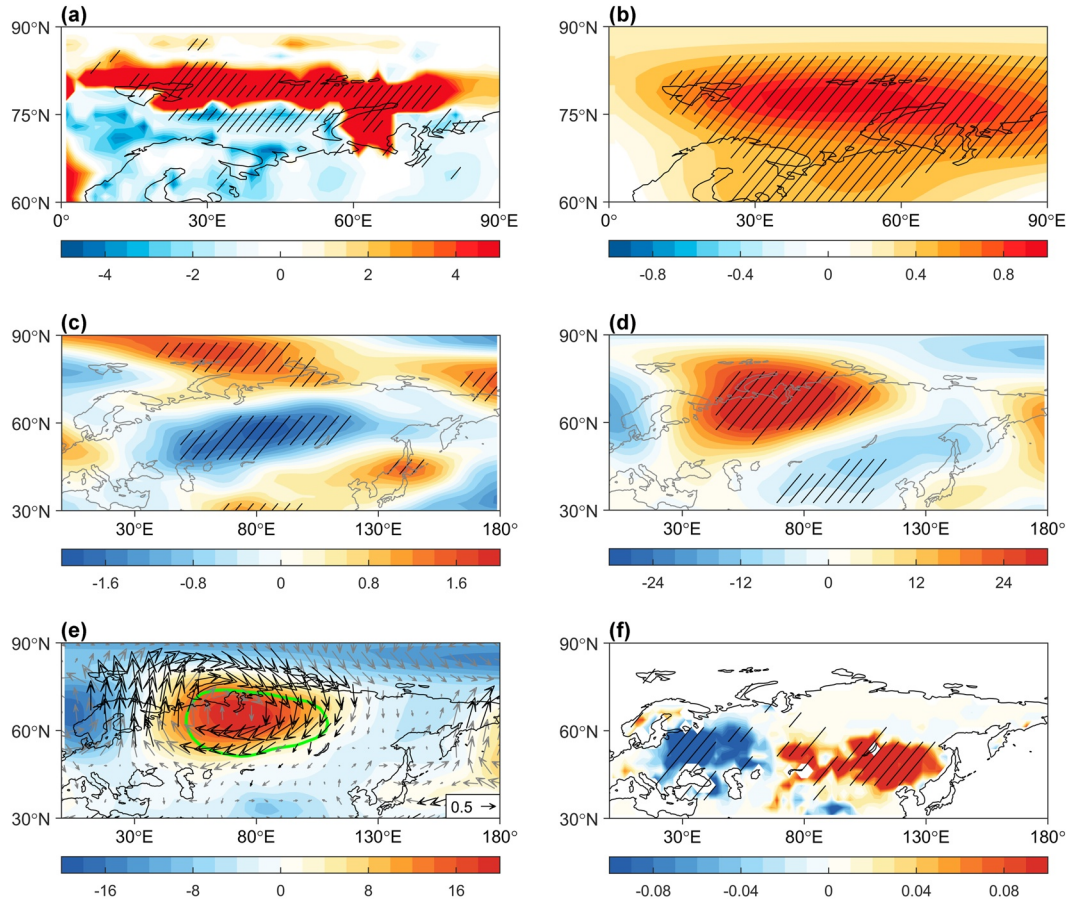

Figure 10. Anomalies of (a) turbulent heat flux, (b) mean air temperature of 1,000–200 hPa, 500-hPa (c) zonal wind (m s^{-1}) and (d) geopotential height (gpm), (e) 850-hPa wind (vectors; m s^{-1}) and geopotential height (shading; gpm), and (f) snow cover fraction obtained by regression against the sign-reversed SICI. Hatching, green circle, and black vectors denote anomalies significant at the 95% confidence level.

with those related to PC1 (Figure S4 in Supporting Information S1), confirming the crucial role of the influencing factors identified by this study in forming the dipole pattern of the snow cover variability over Eurasia during late autumn.

5. Summary and Discussion

This study investigated the influencing factors and the associated physical processes for the formation of the zonal dipole pattern of the Eurasian snow cover variability during late autumn. An EOF analysis suggested that the first EOF mode of the Eurasian snow cover variability can be used to represent the dipole mode. Further analyses indicated that the large-scale atmospheric circulation anomalies play a major role in forming the dipole snow cover variability. Then, we investigated the contributors to the circulation anomalies by considering the effects of the atmospheric teleconnection patterns, SST anomalies and sea ice variations. The results showed that the dipole snow cover variability has close correlations with the teleconnection patterns of EA, EAWR, and SCAND. The anomalous circulations associated with these teleconnections could induce the air temperature and snowfall anomalies that directly shape snow cover variability. In addition, we found that a dipole pattern of the SST anomalies over the North Atlantic could affect the Eurasian snow cover variability through exciting a Rossby wave train prevailing over Eurasia. Moreover, the sea ice concentration variations over the Barents Sea could alter the meridional temperature gradient between the mid and high latitudes, which further modulates the atmospheric circulation anomalies over Eurasia and hence influence the snow cover variability. Finally, we explored the synthetic effects of the influencing factors identified above, and found that they can jointly explain about 66% of the snow cover variability related to the dipole pattern.

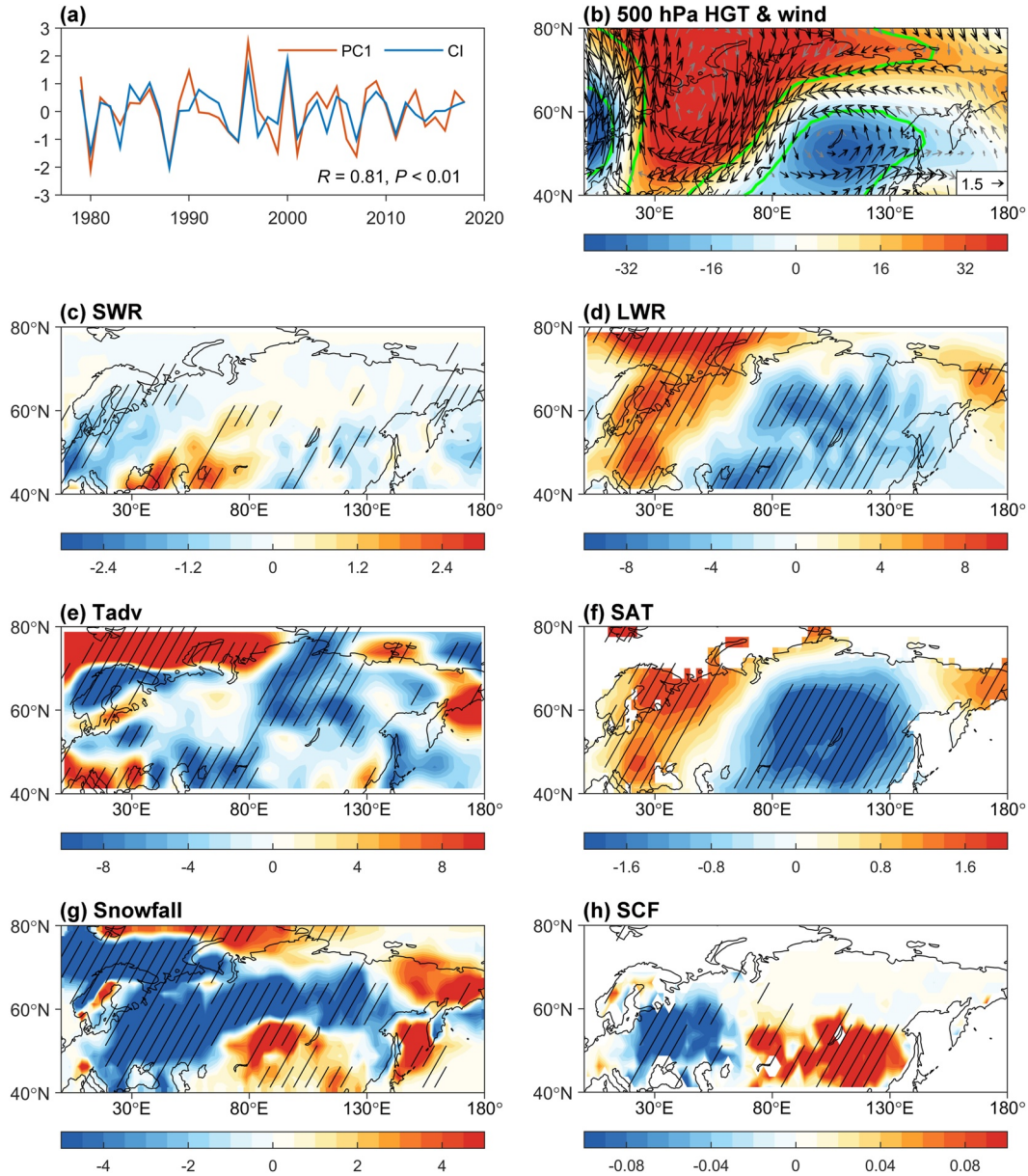

Figure 11. Time series of PC1 and CI (a). Anomalies of (b) geopotential height (shading; gpm) and wind (vectors; m s^{-1}) at 500 hPa, (c) downward shortwave radiation flux (W m^{-2}), (d) downward longwave radiation flux (W m^{-2}), (e) thermal advection (°C), (f) surface air temperature (°C), (g) snowfall (mm), and (h) snow cover fraction obtained by regression onto the CI. The black vectors and the areas circled by green solid lines in (b) and the hatched areas in (c–h) denote the anomalies significant at the 95% confidence level.

In this study, we showed that the anomalous atmospheric circulations related to the teleconnection patterns exert notable influence on the dipole snow cover variability over Eurasia. Note that there is an interaction between snow cover variability and atmospheric circulation anomalies (Henderson et al., 2018; Xu & Dirmeyer, 2013). This implies that the close correlations between snow cover and teleconnections may also denote the effects of snow cover variability on anomalous circulations. For example, previous studies indicated that the Eurasian autumn snow cover can affect the AO and NAO in the following winter (Gastineau et al., 2017; Han & Sun, 2018; Santolaria-Otín et al., 2020; Wegmann et al., 2020). Here, we found the dipole snow cover variability has no significant correlation with the simultaneous AO and NAO (Table 1), suggesting that the variations of AO and NAO may not be affected by the simultaneous dipole snow cover variability. In addition, the EA, EAWR, and SCAND are the stationary large-scale anomalous circulation patterns that are forced and maintained

by the feedback forcing from transient eddies over the North Atlantic (Bueh & Nakamura, 2007; Feldstein & Franzke, 2017; Kim et al., 2021; Lim, 2015). This means that the occurrence of the teleconnection patterns may be independent of the Eurasian snow cover variability. Therefore, the intimate connection between the snow cover variability and teleconnection patterns may mainly stem from the impact of the latter on the former. It is difficult to quantitatively isolate the cause and effect between snow cover variability and circulation anomalies, further numerical experiments are required to address this issue.

Data Availability Statement

The snow cover data used in this study are available at NSIDC (Brodzik & Armstrong, 2013) and JASMES (Hori et al., 2017). The monthly SST and sea ice concentration data were derived from NOAA ERSST v5 (Huang et al., 2017) and HadISST1 (Rayner et al., 2003), respectively. The SAT data was obtained from the CRU TS v4.03 (Harris et al., 2020). In addition, the atmospheric variables were provided by the NCEP-NCAR Reanalysis 1 (Kalnay et al., 1996), JRA-55 (Kobayashi et al., 2015), and ERA5 (Hersbach et al., 2019).

Acknowledgments
This work was jointly supported by the National Key Research and Development Program of China (2022YFF0801603), and the Startup Foundation for Introducing Talent of NUIST (2022r002).

References

Ao, J., & Sun, J. Q. (2016). Connection between November snow cover over Eastern Europe and winter precipitation over East Asia. *International Journal of Climatology*, *36*(5), 2396–2404. https://doi.org/10.1002/joc.4484

Bailey, H., Hubbard, A., Klein, E. S., Mustonen, K.-R., Akers, P. D., Marttila, H., & Welker, J. M. (2021). Arctic sea-ice loss fuels extreme European snowfall. *Nature Geoscience*, *14*(5), 283–288. https://doi.org/10.1038/s41561-021-00719-y

Barnett, T. P., Dumenil, L., Schlese, U., & Roeckner, E. (1988). The effect of Eurasian snow cover on global climate. *Science*, *239*(4839), 504–507. https://doi.org/10.1126/science.239.4839.504

Barnston, A. G., & Livezey, R. E. (1987). Classification, seasonality and persistence of low-frequency atmospheric circulation patterns. *Monthly Weather Review*, *115*(6), 1083–1126. https://doi.org/10.1175/1520-0493(1987)115<1083:CSAPOL>2.0.CO;2

Brodzik, M. J., & Armstrong, R. (2013). Northern hemisphere EASE-grid 2.0 weekly snow cover and sea ice extent, Version 4 [Dataset]. NASA National Snow and Ice Data Center Distributed Active Archive Center. https://doi.org/10.5067/P7O0HGJLYUQU

Bueh, C., & Nakamura, H. (2007). Scandinavian pattern and its climatic impact. *Quarterly Journal of the Royal Meteorological Society*, *133*(629), 2117–2131. https://doi.org/10.1002/qj.173

Cai, M., Yang, S., Den, V., Dool, H., & Kousky, V. (2007). Dynamical implications of the orientation of atmospheric eddies: A local energetics perspective. *Tellus A*, *59*(1), 127–140. https://doi.org/10.1111/j.1600-0870.2006.00213.x

Chen, S., Wu, R., Chen, W., Hu, K. M., & Yu, B. (2020). Structure and dynamics of a springtime atmospheric wave train over the North Atlantic and Eurasia. *Climate Dynamics*, *54*(11–12), 5111–5126. https://doi.org/10.1007/s00382-020-05274-7

Chen, S., Wu, R., Chen, W., Song, L., Cheng, W., & Shi, W. (2021). Weakened impact of autumn Arctic sea ice concentration change on the subsequent winter Siberian High variation around the late-1990s. *International Journal of Climatology*, *41*(S1), E2700–E2717. https://doi.org/10.1002/joc.6875

Chen, S., Wu, R., & Liu, Y. (2016). Dominant modes of interannual variability in Eurasian surface air temperature during boreal spring. *Journal of Climate*, *29*(3), 1109–1125. https://doi.org/10.1175/JCLI-D-15-0524.1

Choi, Y. W., & Ahn, J. B. (2019). Possible mechanisms for the coupling between late spring sea surface temperature anomalies over tropical Atlantic and East Asian summer monsoon. *Climate Dynamics*, *53*(11), 6995–7009. https://doi.org/10.1007/s00382-019-04970-3

Clark, M. P., Serreze, M. C., & Robinson, D. A. (1999). Atmospheric controls on Eurasian snow extent. *International Journal of Climatology*, *19*(1), 27–40. https://doi.org/10.1002/(SICI)1097-0088(199901)19:1<27::AID-JOC346>3.0.CO;2-N

Cohen, J., Agel, L., Barlow, M., Garfinkel, C. I., & White, I. (2021). Linking Arctic variability and change with extreme winter weather in the United States. *Science*, *373*(6559), 1116–1121. https://doi.org/10.1126/science.abi9167

Cohen, J., Barlow, M., Kushner, P., & Saito, K. (2007). Stratosphere-troposphere coupling and links with Eurasian land-surface variability. *Journal of Climate*, *20*(21), 5335–5343. https://doi.org/10.1175/2007JCLI1725.1

Cohen, J., & Rind, D. (1991). The effect of snow cover on the climate. *Journal of Climate*, *4*(7), 689–706. https://doi.org/10.1175/1520-0442(1991)004<0689:TEOSCO>2.0.CO;2

Dai, A. G., Luo, D. H., Song, M. R., & Liu, J. P. (2019). Arctic amplification is caused by sea-ice loss under increasing CO_2. *Nature Communications*, *10*(1), 121. https://doi.org/10.1038/s41467-018-07954-9

Douville, H., Peings, Y., & Saint-Martin, D. (2017). Snow-(N)AO relationship revisited over the whole twentieth century. *Geophysical Research Letters*, *44*(1), 569–577. https://doi.org/10.1002/2016GL071584

Duchon, C. E. (1979). Lanczos filtering in one and two dimensions. *Journal of Applied Meteorology and Climatology*, *18*(8), 1016–1022. https://doi.org/10.1175/1520-0450(1979)018,1016:LFIOAT.2.0.CO;2

Feldstein, S., & Franzke, C. (2017). Atmospheric teleconnection patterns. In C. Franzke & T. O'Kane (Eds.), *Nonlinear and stochastic climate dynamics* (pp. 54–104). Cambridge University Press. https://doi.org/10.1017/9781316339251.004

Furtado, J. C., Cohen, J. L., Butler, A. H., Riddle, E. E., & Kumar, A. (2015). Eurasian snow cover variability and links to winter climate in the CMIP5 models. *Climate Dynamics*, *45*(9–10), 2591–2605. https://doi.org/10.1007/s00382-015-2494-4

Furtado, J. C., Cohen, J. L., & Tziperman, E. (2016). The combined influences of autumnal snow and sea ice on Northern Hemisphere winters. *Geophysical Research Letters*, *43*(7), 3478–3485. https://doi.org/10.1002/2016gl068108

Gao, T., Yu, J., & Paek, H. (2017). Impacts of four northern-hemisphere teleconnection patterns on atmospheric circulations over Eurasia and the Pacific. *Theoretical and Applied Climatology*, *129*(3–4), 815–831. https://doi.org/10.1007/s00704-016-1801-2

Gao, Y., Sun, J., Li, F., He, S., Stein, S., Yan, Q., et al. (2015). Arctic sea ice and Eurasian climate: A review. *Advances in Atmospheric Sciences*, *32*(1), 92–114. https://doi.org/10.1007/s00376-014-0009-6

Gastineau, G., García-Serrano, J., & Frankignoul, C. (2017). The influence of autumnal Eurasian snow cover on climate and its link with Arctic sea ice cover. *Journal of Climate*, *30*(19), 7599–7619. https://doi.org/10.1175/JCLI-D-16-0623.1

Groisman, P. Y., Karl, T. R., & Knight, R. W. (1994). Observed impact of snow cover on the heat balance and the rise of continental spring temperatures. *Science*, *263*(5144), 198–200. https://doi.org/10.1126/science.263.5144.198

Halder, S., & Dirmeyer, P. A. (2017). Relation of Eurasian snow cover and Indian summer monsoon rainfall: Importance of the delayed hydrological effect. *Journal of Climate*, *30*(4), 1273–1289. https://doi.org/10.1175/JCLI-D-16-0033.1

Han, S., & Sun, J. (2018). Impacts of autumnal Eurasian snow cover on predominant modes of boreal winter surface air temperature over Eurasia. *Journal of Geophysical Research: Atmospheres*, *123*(18), 10076–10091. https://doi.org/10.1029/2018JD028443

Han, S., & Sun, J. (2021). Connection between the November snow cover over northeast Asia and the following January precipitation in southern China. *International Journal of Climatology*, *41*(4), 2553–2567. https://doi.org/10.1002/joc.6974

Harris, I., Osborn, T. J., Jones, P., & Lister, D. (2020). Version 4 of the CRU TS monthly high-resolution gridded multivariate climate dataset [Dataset]. Scientific Data, *7*(1), 109. https://doi.org/10.5285/10d3e3640f004c578403419aac167d82

Henderson, G. R., & Leathers, D. J. (2010). European snow cover extent variability and associations with atmospheric forcings. *International Journal of Climatology*, *30*(10), 1440–1451. https://doi.org/10.1002/joc.1990

Henderson, G. R., Peings, Y., Furtado, J. C., & Kushner, P. J. (2018). Snow–atmosphere coupling in the northern hemisphere. *Nature Climate Change*, *8*(11), 954–963. https://doi.org/10.1038/s41558-018-0295-6

Hersbach, H., Bell, B., Berrisford, P., Biavati, G., Horányi, A., Sabater, M., et al. (2019). ERA5 monthly averaged data on pressure levels from 1959 to present [Dataset]. Copernicus Climate Change Service (C3S) Climate Data Store (CDS). https://doi.org/10.24381/cds.6860a573

Holton, J. R. (1992). *An introduction to dynamic meteorology*. Academic Press.

Hori, M., Sugiura, K., Kobayashi, K., Aoki, T., Tanikawa, T., Kuchiki, K., et al. (2017). A 38-year (1978–2015) Northern Hemisphere daily snow cover extent product derived using consistent objective criteria from satellite-borne optical sensors [Dataset]. Remote Sensing of Environment, *191*, 402–418. https://doi.org/10.1016/j.rse.2017.01.023

Huang, B., Thorne, P. W., Banzon, V. F., Boyer, T., Chepurin, G., Lawrimore, J. H., et al. (2017). Extended reconstructed sea surface temperature, version 5 (ERSSTv5): Upgrades, validations, and intercomparisons [Dataset]. Journal of Climate, *30*(20), 8179–8205. https://doi.org/10.1175/JCLI-D-16-0836

Kalnay, E., Kanamitsu, M., Kistler, R., Collins, W., Deaven, D., Gandin, L., et al. (1996). The NCEP/NCAR 40-year reanalysis project [Dataset]. Bulletin of the American Meteorological Society, *77*(3), 437–471. https://doi.org/10.1175/1520-0477(1996)077<0437:tnyrp>2.0.co;2

Kim, M., Yoo, C., Sung, M., & Lee, S. (2021). Classification of wintertime atmospheric teleconnection patterns in the northern hemisphere. *Journal of Climate*, *34*(5), 1847–1861. https://doi.org/10.1175/JCLI-D-20-0339.1

Kim, Y., Kim, K. Y., & Kim, B. M. (2013). Physical mechanisms of European winter snow cover variability and its relationship to the NAO. *Climate Dynamics*, *40*(7–8), 1657–1669. https://doi.org/10.1007/s00382-012-1365-5

Kobayashi, S., Ota, Y., Harada, Y., Ebita, A., Moriya, M., Onoda, H., et al. (2015). The JRA-55 reanalysis: General specifications and basic characteristics [Dataset]. Journal of the Meteorological Society of Japan, *93*(1), 5–48. https://doi.org/10.2151/jmsj.2015-001

Lau, N. C. (1988). Variability of the observed midlatitude storm tracks in relation to low-frequency changes in the circulation pattern. *Journal of the Atmospheric Sciences*, *45*(19), 2718–2743. https://doi.org/10.1175/1520-0469(1988)045<2718:VOTOMS>2.0.CO;2

Li, J., Li, F., & Wang, H. J. (2020). Subseasonal prediction of winter precipitation in southern China using the early November snowpack over the Urals. *Atmospheric and Oceanic Science Letters*, *13*(6), 534–541. https://doi.org/10.1080/16742834.2020.1824547

Lim, Y. K. (2015). The East Atlantic/West Russia (EA/WR) teleconnection in the North Atlantic: Climate impact and relation to Rossby wave propagation. *Climate Dynamics*, *44*(11–12), 3211–3222. https://doi.org/10.1007/s00382-014-2381-4

Liu, Y., Wang, L., Zhou, W., & Chen, W. (2014). Three Eurasian teleconnection patterns: Spatial structures, temporal variability, and associated winter climate anomalies. *Climate Dynamics*, *42*(11–12), 2817–2839. https://doi.org/10.1007/s00382-014-2163-z

Luo, X., & Wang, B. (2019). How autumn Eurasian snow anomalies affect East Asian winter monsoon: A numerical study. *Climate Dynamics*, *52*(1–2), 69–82. https://doi.org/10.1007/s00382-018-4138-y

North, G. R., Bell, T. L., Cahalan, R. F., & Moeng, F. J. (1982). Sampling errors in the estimation of empirical orthogonal functions. *Monthly Weather Review*, *110*(7), 699–706. https://doi.org/10.1175/1520-0493(1982)110,0699:SEITEO.2.0.CO;2

Peings, Y., Brun, E., Mauvais, V., & Douville, H. (2013). How stationary is the relationship between Siberian snow and Arctic Oscillation over the 20th century? *Geophysical Research Letters*, *40*(1), 183–188. https://doi.org/10.1029/2012GL054083

Peings, Y., & Douville, H. (2010). Influence of the Eurasian snow cover on the Indian summer monsoon variability in observed climatologies and CMIP3 simulations. *Climate Dynamics*, *34*(5), 643–660. https://doi.org/10.1007/s00382-009-0565-0

Rayner, N. A., Parker, D. E., Horton, E. B., Folland, C. K., Alexander, L. V., Rowell, D. P., et al. (2003). Global analyses of sea surface temperature, sea ice, and night marine air temperature since the late nineteenth century [Dataset]. Journal of Geophysical Research, *108*(D14), 4407. https://doi.org/10.1029/2002jd002670

Santolaria-Otín, M., García-Serrano, J., Ménégoz, M., & Bech, J. (2020). On the observed connection between Arctic sea ice and Eurasian snow in relation to the winter North Atlantic Oscillation. *Environmental Research Letters*, *15*(12), 124010. https://doi.org/10.1088/1748-9326/abad57

Seager, R., Kushnir, Y., Nakamura, J., Ting, M., & Naik, N. (2010). Northern hemisphere winter snow anomalies: ENSO, NAO and the winter of 2009/10. *Geophysical Research Letters*, *37*(14), L14703. https://doi.org/10.1029/2010GL043830

Song, Y., Chen, H., & Yang, J. (2022). The dominant modes of boreal spring land surface temperature over Western Eurasia and their possible linkages with large-scale atmospheric teleconnection patterns. *Journal of Geophysical Research: Atmospheres*, *127*(4), e2021JD035720. https://doi.org/10.1029/2021JD035720

Sun, C. H., Zhang, R. N., Li, W. J., Zhu, J. S., & Yang, S. (2019). Possible impact of North Atlantic warming on the decadal change in the dominant modes of winter Eurasian snow water equivalent during 1979-2015. *Climate Dynamics*, *53*(9–10), 5203–5213. https://doi.org/10.1007/s00382-019-04853-7

Sun, J., Liu, S., Cohen, J., & Yu, S. (2022). Influence and prediction value of Arctic sea ice for spring Eurasian extreme heat events. *Communications Earth & Environment*, *3*(1), 172. https://doi.org/10.1038/s43247-022-00503-9

Takaya, K., & Nakamura, H. (1997). A formulation of a wave activity flux for stationary Rossby waves on a zonally varying basic flow. *Geophysical Research Letters*, *24*(23), 2985–2988. https://doi.org/10.1029/97GL03094

Takaya, K., & Nakamura, H. (2001). A formulation of a phase-independent wave activity flux for stationary and migratory quasi-geostrophic eddies on a zonally varying basic flow. *Journal of the Atmospheric Sciences*, *58*(6), 608–627. https://doi.org/10.1175/1520-0469(2001)058,0608:AFOAPI.2.0.CO;2

Thompson, D. W., & Wallace, J. M. (1998). The Arctic Oscillation signature in the wintertime geopotential height and temperature fields. *Geophysical Research Letters*, *25*(9), 1297–1300. https://doi.org/10.1029/98GL00950

Wallace, J. M., & Gutzler, D. S. (1981). Teleconnections in the geopotential height field during the Northern Hemisphere winter. *Monthly Weather Review*, *109*(4), 784–812. https://doi.org/10.1175/1520-0493(1981)109<0784:TITGHF>2.0.CO;2

Watanabe, M. (2004). Asian jet waveguide and a downstream extension of the North Atlantic oscillation. *Journal of Climate*, *17*(24), 4674–4691. https://doi.org/10.1175/JCLI-3228.1

Wegmann, M., Rohrer, M., Santolaria-Otín, M., & Lohmann, G. (2020). Eurasian autumn snow link to winter North Atlantic Oscillation is strongest for Arctic warming periods. *Earth System Dynamics*, *11*(2), 509–524. https://doi.org/10.5194/esd-11-509-2020

Wu, B. Y., Yang, K., & Zhang, R. H. (2009). Eurasian snow cover variability and its association with summer rainfall in China. *Advances in Atmospheric Sciences*, *26*(1), 31–44. https://doi.org/10.1007/s00376-009-0031-2

Wu, R., & Kirtman, B. P. (2007). Observed relationship of spring and summer East Asian rainfall with winter and spring Eurasian snow. *Journal of Climate*, *20*(7), 1285–1304. https://doi.org/10.1175/JCLI4068.1

Wu, R., Yang, S., Liu, S., Sun, L., Lian, Y., & Gao, Z. (2011). Northeast China summer temperature and North Atlantic SST. *Journal of Geophysical Research*, *116*(D16), D16116. https://doi.org/10.1029/2011JD015779

Xu, B., Chen, H., Gao, C., Zhou, B., Sun, S., & Zhu, S. (2019). Regional response of winter snow cover over the Northern Eurasia to late autumn Arctic sea ice and associated mechanism. *Atmospheric Research*, *222*, 100–113. https://doi.org/10.1016/j.atmosres.2019.02.010

Xu, L., & Dirmeyer, P. (2013). Snow–atmosphere coupling strength. Part II: Albedo effect versus hydrological effect. *Journal of Hydrometeorology*, *14*(2), 404–418. https://doi.org/10.1175/JHM-D-11-0103.1

Yang, H., & Fan, K. (2021). Strengthened impacts of November snow cover over Siberia on the out of-phase change in the Siberian high between December and January since 2000 and implication for intraseasonal climate prediction. *Frontiers of Earth Science*, *9*, 748484. https://doi.org/10.3389/feart.2021.748484

Ye, K. (2019). Interannual variability of March snow mass over Northern Eurasia and its relation to the concurrent and preceding surface air temperature, precipitation and atmospheric circulation. *Climate Dynamics*, *52*(5–6), 2813–2836. https://doi.org/10.1007/s00382-018-4297-x

Ye, K., & Wu, R. (2017). Autumn snow cover variability over northern Eurasia and roles of atmospheric circulation. *Advances in Atmospheric Sciences*, *34*(7), 847–858. https://doi.org/10.1007/s00376-017-6287-z

Zhang, R., Zhang, R. H., & Zuo, Z. (2017). Impact of Eurasian spring snow decrement on East Asian summer precipitation. *Journal of Climate*, *30*(9), 3421–3437. https://doi.org/10.1175/JCLI-D-16-0214.1

Zhang, T., Wang, T., Feng, Y., Li, X., & Krinner, G. (2021). An emerging impact of Eurasian spring snow cover on summer rainfall in Eastern China. *Environmental Research Letters*, *16*(5), 054012. https://doi.org/10.1088/1748-9326/abf688

Zhang, T., Wang, T., Krinner, G., Wang, X., Gasser, T., Peng, S., et al. (2019). The weakening relationship between Eurasian spring snow cover and Indian summer monsoon rainfall. *Science Advances*, *5*(3), eaau8932. https://doi.org/10.1126/sciadv.aau893

Zhang, T., Wang, T., Zhao, Y., Xu, C., Feng, Y., & Liu, D. (2021). Drivers of Eurasian spring snow-cover variability. *Journal of Climate*, *34*(6), 2037–2052. https://doi.org/10.1175/JCLI-D-20-0413